Electron loss and single and double capture of C^{3+} and O^{5+} ions in collisions with noble gases

W. S. Melo,* M. M. Sant'Anna, A. C. F. Santos, G. M. Sigaud, and E. C. Montenegro
Departamento de Física, Pontifícia Universidade Católica do Rio de Janeiro, Caixa Postal 38071, Rio de Janeiro 22452-970, RJ, Brazil
(Received 26 January 1999)

Cross sections for the processes of projectile electron loss and single and double capture of C^{3+} and O^{5+} projectile ions impinging on He, Ne, Ar, Kr, and Xe targets were measured in the energy range of 1.0–3.5 MeV. The measured cross sections present a strong saturation as the target atomic number increases, for all the systems and collision channels studied. The single-capture data are compared with calculations based on a semiclassical model and on the eikonal approximation, both presenting a good general agreement with the experiment. In the case of electron loss, the observed saturation is in accordance with previous measurements for He^+ projectiles, and is present in the first-order calculations for the antiscreening contribution but not in those for the screening. This is due to the fact that, for heavy target atoms, the screening mode can be highly nonperturbative. Calculations for the screening contribution to the electron loss, based on the free-collision model, together with first-order results for the antiscreening, are compared with the experimental data, presenting good agreement in most cases. However, this comparison also shows that one has to include other competitive channels in order to give a better description of the collision. [S1050-2947(99)04208-0]

PACS number(s): 34.50.Fa, 52.20.Hv

I. INTRODUCTION

In collisions between multiply charged dressed ions and neutral atoms there is a multiplicity of collision channels acting simultaneously, which result in single- or multiple-electron transitions within and between the participating systems. Some of these channels include the single or multiple ionization of the projectile and of the target atom, followed — or not — by the capture of one — or more — target electrons by the incoming ion.

The simultaneous occurrence of these processes renders difficult a comprehensive theoretical description of the collision. Only in the simplest cases can single-channel analyses be used to describe properly the experimental results. However, for a rather large variety of combinations of collision partners and velocities, the probabilities for several of these processes are of the same order of magnitude and, thus, have to be considered simultaneously, since they are no longer independent. This is the case, for example, when one wants to study the projectile electron loss for such a combination of projectile charge state and velocity so that the capture channel may become very important as compared to the loss. In this situation, the coupling of these channels has to be taken into account for a correct description of the problem [1]. There are cases where even the double-capture channel can play an important role for sufficiently low velocities. Thus, a detailed understanding of each of these mechanisms is mandatory to a satisfactory description of the collision.

In the case of projectile electron loss, it has been well established that this process is governed by two competing mechanisms, the so-called screening and antiscreening effects [2,3], whose behavior for light targets is conveniently described by first-order models, such as the plane-wave Born approximation (PWBA) [3,4]. This does not hold, however, for heavier targets, when the dominant Z_2^2 dependence of the screening contribution predicted by the PWBA for the total cross section, where Z_2 is the target atomic number, is not confirmed by the experiment as, for example, in the data presented by Sant'Anna *et al.* [5]. These authors measured total electron-loss cross sections for He^+ projectiles as a function of Z_2 and observed a strong saturation for $Z_2 \geqslant 10$, which is present in the first-order calculations for the antiscreening contribution but not in those for the screening.

More recently, Sigaud *et al.* [6] also reported on a similar saturation with increasing target atomic number in measurements of the cusp yields of the electron loss to the continuum (ELC) process for 1.0 MeV He^+ projectiles impinging upon atomic and molecular gaseous targets.

Such a saturation for the screening was already observed experimentally in the excitation of highly charged projectiles in collisions with neutral targets [7–12]. Several theoretical attempts to describe those experiments, using either nonperturbative or second-order approaches, have been made, sometimes quite successfully [7,8,11–16].

The failure of first-order perturbative treatments of the screening contribution to the electron loss of dressed ions by heavy neutral atoms is due to the fact that, in this case, there can be a significant contribution from collisions occurring at small impact parameters. This implies that the interaction between the projectile active electron and the target nucleus—screened by the target electrons to different degrees — can be highly nonperturbative [17]. On the other hand, the antiscreening contribution can be conveniently treated perturbatively since it is due to a sum of several electron-electron interactions [3].

Nonperturbative calculations, using the coupled-channel method, for the screening contribution to the total electron-loss cross sections were presented by Grande *et al.* [18] for the He^+ data of Ref. [5]. These calculations were only partially successful since, although a great improvement was obtained when compared to first-order results, this model

*Present address: Instituto de Física, Universidade Federal Fluminense, Niterói, RJ, Brazil.

was still unable to explain completely the experimental data for the heaviest targets.

In a recent paper, Voitkiv *et al.* [19] compared the same data of Ref. [5] with calculations using the sudden approximation. These authors showed the importance of the target ionization channel to a more correct description of the He^+-loss process. However, there are no calculations as sophisticated as these applied to the electron loss of more complex, multielectron projectile ions.

In the case of the single-capture channel, a similar saturation was also reported by Anholt *et al.* [20] for C ions, with energies ranging from 10 to 42 MeV, colliding with gaseous and solid targets. These authors compared their data with calculations based on the eikonal approximation [21–23], with reasonably good results. However, the theoretical description of the capture process in the low- to intermediate-velocity regime — i.e., near the limit of validity of perturbative approaches — is not an easy task.

In this work total cross sections for the projectile electron-loss and single- and double-capture processes in collisions of C^{3+} and O^{5+} with He, Ne, Ar, Kr, and Xe targets, with energies ranging from 1.0 to 3.5 MeV, are reported. For the projectile-loss channel, the main objective is to study the dependence of the total cross sections with the target atomic number in order to have a more detailed insight into the role played by screening and antiscreening contributions beyond the perturbative limit. For this purpose, calculations for the screening contribution using the free-collision model [24] are presented and, together with first-order calculations for the antiscreening [25], are compared with the electron-loss data, including the previous ones for He^+ projectiles from Ref. [5]. These calculations were also performed for He^+ and C^{3+} projectiles impinging upon atomic hydrogen targets and are compared with experimental results recently reported by Sant'Anna *et al.* [26]. In the case of the single capture, the data presented here are compared to two different models, the eikonal approximation [23] and the semiclassical model of Ben-Itzhak *et al.* [27].

The paper is arranged as follows: in Sec. II the experimental setup and data analysis are briefly described and the experimental results are presented; in Sec. III the calculations for the screening and antiscreening contributions to the electron loss are presented and compared with the data; in Sec. IV the calculations for the single-capture channel are compared to the data; and, finally, in Sec. V a summary of the work is presented. In the Appendix, the analytical expression, based on the semiclassical model of Ben-Itzhak *et al.* used in the single-capture calculation is deduced.

II. EXPERIMENT

The C^{3+} and O^{5+} beams, with energies ranging from 1.0 to 3.5 MeV, were obtained from C^+ and O^+ or O^{2+} beams, provided by the 4.0 MV Van de Graaff accelerator of the Catholic University of Rio de Janeiro, which passed through a gas stripper. The experimental setup is essentially the same used in Refs. [5,28,29] for singles measurements, so that only its most important features will be described here. The beam is charge and energy analyzed by two magnets before entering the experimental beamline, where it is collimated to a spot smaller than 1 mm^2. Great care was taken to reduce slit scattering. After traversing the target chamber, which is a gas cell with an effective length of 7.2 cm [30], where it collides with high-purity (better than 99.999%) He, Ne, Ar, Kr, and Xe gas targets, the beam was charge-state analyzed by a third magnet. Four charge states, corresponding to the loss and single- and double-capture channels, besides the impinging charge state, were detected in a *x-y* position-sensitive microchannel plate detector, located $\sim$4.5 m downstream from the collision chamber. This detector was also used to locate any spurious beams that might be created by charge-changing collisions of the main beam with the residual gas inside the beamline before the gas cell. In order to separate these undesired spurious beams from the main one, the beam passes through a cleaning magnet, located at $\sim$0.2 m upstream from the center of the collision chamber.

TABLE I. Total electron-loss cross sections for C^{3+} (Mb).

E (MeV)	He	Ne	Ar	Kr	Xe
1.00	6.14±0.74	12.0±1.4	13.6±1.6	7.24±0.87	21.2±2.5
1.50	12.0±1.4	17.7±2.1	37.5±4.5	21.3±2.5	50.0±6.0
2.00	15.5±1.9	27.8±3.3	66.8±8.0	45.3±5.4	78.9±9.5
2.50	16.7±2.0	39.6±4.8	82.3±9.9	72.8±8.7	97.4±11.7
3.00	16.6±2.0	47.8±5.7	87.1±10.5	86.6±10.4	105±13
3.50	16.9±2.0	51.2±6.1	87.4±10.5	95.9±11.5	110±13

Total absolute electron-loss and single- and double-capture cross sections were obtained by the growth-rate method [1]. The single-electron capture is the most important charge-changing channel for these projectiles at the lowest velocities considered here — the cross sections may reach some thousands of Mb. Thus, the absolute pressures used in the gas cell, measured by an absolute capacitive manometer (MKS-Baratron), were always smaller than 2.0 mTorr to guarantee single-collision conditions.

The experimental results are shown in Tables I–VI for the projectile electron-loss (Tables I and II) and single-capture (Tables III and IV) and double-capture (Tables V and VI) channels, as functions of the projectile energy and the target atomic number, for the C^{3+} and O^{5+} projectiles, respectively. The main sources of uncertainties are the impurities in the gas targets due to the gas-admittance system ($\sim$1 $-$3%), the determination of the length of the gas cell ($\sim$5%), counting statistics ($\sim$5%), and interference of spurious beams ($\sim$1%).

III. TOTAL ELECTRON LOSS AND THE TARGET ATOMIC NUMBER: SCREENING, FREE-COLLISION MODEL, AND ANTISCREENING

The calculations for the screening contribution to the electron loss were carried out using an extension of the free-

TABLE II. Total electron-loss cross sections for O^{5+} (Mb).

E (MeV)	He	Ne	Ar	Kr	Xe
2.00	1.34±0.16	0.82±0.10			
2.50	2.24±0.27	2.37±0.28	4.35±0.52	2.54±0.30	5.04±0.60
3.00	2.72±0.33	3.50±0.42	10.1±1.2	5.22±0.63	12.8±1.5
3.50	3.70±0.44	5.78±0.69	18.5±2.2	10.4±1.2	19.8±2.4

TABLE III. Total single-electron capture cross sections for C^{3+} (Mb).

E (MeV)	He	Ne	Ar	Kr	Xe
1.00	346±42	465±56	763±92	965±116	1004±120
1.50	176±21	264±32	405±49	440±53	416±50
2.00	103±12	199±24	205±25	235±28	230±28
2.50	66.5±8.0	133±16	140±17	140±17	127±15
3.00	38.3±4.6	100±12	72.9±8.7	86.5±10.4	96.8±11.6
3.50	29.7±3.6	74.1±8.9	42.2±5.1	42.1±5.1	61.6±7.4

collision classical-impulse approximation [31] presented by Riesselmann *et al.* [24]. These last authors applied this model to evaluate the cross sections for the electron loss of $H(1s)$ and the single- and double-electron loss of H^- projectiles by gaseous atomic targets. Here an extension to heavier projectiles is presented. In this model, the electron of the projectile is treated as a free electron, whose velocity is the vector sum of the velocity of the projectile center of mass and that of the electron bound to the projectile. The basic assumption is, then, that the electron is scattered by a target atom with the same scattering cross section of a free electron with that added velocity. The momentum transferred to the projectile-active electron during the collision must be such that it acquires enough energy to be ionized. Thus, for kinematic reasons, the free-electron scattering angle must be larger than a critical value, which depends on the kinematic quantities of the collision.

In Ref. [24] a further restriction is made, that is, that the calculations be limited to values of the projectile velocity which are greater than the root-mean-square velocity of the active electron in the projectile. This approximation is also used here, and leads to an important feature of the application of the model to the calculation of the screening contribution, since it presents a threshold at the same projectile velocity where the onset for the antiscreening occurs. However, it also limits the application of the model to energies greater than 0.4, 1.4, and 4.0 MeV for the He^+, C^{3+}, and O^{5+} projectiles, respectively.

Following the notation of Ref. [24], and within the high-velocity approximation cited above, the expression for the electron-loss cross section as a function of the projectile center-of-mass velocity in the laboratory frame, v_N, $Q(v_N)$, in the free-collision model can be written as

TABLE IV. Total single-electron capture cross sections for O^{5+} (Mb).

E (MeV)	He	Ne	Ar	Kr	Xe
1.00	1117±134	937±112	1944±233	2667±320	2744±329
1.50	754±90	716±86	1120±134	1555±187	1566±188
2.00	498±60	545±65	857±103	988±119	1065±128
2.50	341±41	433±52	681±82	821±96	755±91
3.00	199±24	394±47	402±48	526±63	517±62
3.50	139±17	314±37	357±43	417±50	415±50

TABLE V. Total double-electron capture cross sections for C^{3+} (Mb).

E (MeV)	He	Ne	Ar	Kr	Xe
1.00	37.6±4.5	56.0±6.7	111±13	138±17	103±12
1.50	12.6±1.5	28.4±3.4	30.1±3.6	35.6±4.3	22.5±2.7
2.00	5.39±0.65	15.4±1.8	8.79±1.05	9.40±1.13	10.6±1.3
2.50	1.86±0.22	6.47±0.78	3.55±0.43	4.37±0.52	4.07±0.49
3.00	0.79±0.09	3.70±0.44	0.99±0.12	1.77±0.21	1.59±0.19

$$Q(v_N)=\frac{1}{2}\sum_j \int_0^{\pi}\sin\beta d\beta\int_0^{2\pi}d\phi\int_{\theta_C}^{\pi}\sigma_j(v_N,\theta)\sin\theta d\theta, \tag{1}$$

where θ is the scattering angle of the free electron, θ_C is the critical angle that appears from the kinematic condition mentioned above, β is the angle between the velocities of the projectile in the laboratory frame and of the active electron in the projectile frame, and ϕ is the angle between the plane formed by $\vec{v}_N$ and the electron initial velocity and the plane formed by $\vec{v}_N$ and the electron final velocity, all velocities in the laboratory frame. $\sigma_j(v_N,\theta)$ is the differential electron-scattering cross section for the process j at an angle θ for an electron with velocity v_N incident on a given target. Since in the screening mode the target electrons remain in the ground state, the application of this model to that process is restricted to considering only the elastic scattering of the free electron. This approximation also takes for the electron initial velocity, not the distribution of the electron velocities about the projectile nucleus, but rather the root mean square of this distribution, $u_{\rm rms}$. All these velocities and angles are schematically depicted in Fig. 1.

The evaluation of the cross section using Eq. (1) can be very time consuming, mainly due to the dependence of the critical angle θ_C on the angles β and ϕ [24]. In order to further simplify the calculations, we have used the expansion mentioned in Ref. [24] for $u_{\rm rms}\ll v_N$, so that the critical angle can be rewritten as

$$\theta_C=\frac{u_{\rm rms}}{v_N}[(1+x^2)^{1/2}-x], \tag{2}$$

where $x=\sin\beta\cos\phi$. Substituting this result into Eq. (1), one obtains for the screening contribution to the electron-loss cross section in the high-velocity approximation, $\sigma_{\rm screen}$,

TABLE VI. Total double-electron capture cross sections for O^{5+} (Mb).

E (MeV)	He	Ne	Ar	Kr	Xe
1.00	124±15	226±27	264±32	369±44	385±46
1.50	92.5±11.1	121±15	116±14	161±19	158±19
2.00			71.0±8.5	101±12	127±15
2.50	34.5±4.1	96.5±11.6	52.1±6.3	66.4±8.0	97.5±11.7
3.00	12.9±1.5	81.5±9.8	21.2±2.5	32.5±3.9	68.5±8.2
3.50	7.41±0.89	59.5±7.1	16.4±2.0	30.0±3.6	41.3±5.0

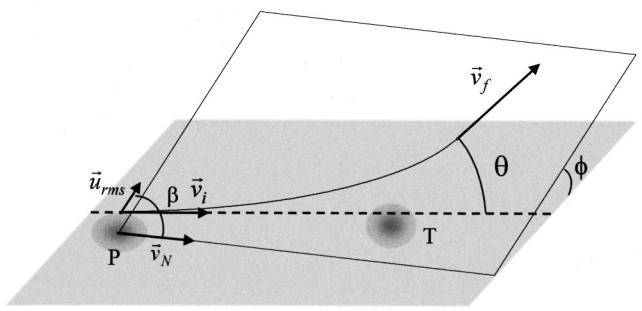

FIG. 1. Schematic view of the velocities and angles used in the free-collision model (see text).

$$\sigma_{\text{screen}}(v_N) = \pi \int_{-1}^{1} dx \int_{\theta_C(x)}^{\pi} \sigma_{\text{el}}(v_N, \theta) \sin\theta d\theta, \qquad (3)$$

where σ_{el} (v_N, θ) is the differential cross section for the elastic scattering of a free electron with velocity v_N. The functions used in the last integration in Eq. (3) are interpolations of the elastic differential electron-scattering cross sections calculated by McCarthy *et al.* [32] using an optical model.

In Fig. 2 the total experimental electron-loss cross sections of He^+ by Ar from Ref. [5] as a function of the collision energy are compared with the total calculated cross sections, which are the sum of the screening contribution, calculated using Eq. (3) above, with the antiscreening contribution calculated using the PWBA extended sum-rule method of Montenegro and Meyerhof [25] (thick solid line). Also shown in Fig. 2 are the total cross sections with the screening contribution calculated using the coupled-channel method from Ref. [18] (dotted line) and the sudden approximation [19] (thick dashed line).

Several points can be noted in this figure. First, the results obtained in the free-collision model are close to those obtained using two other nonperturbative approaches, the coupled-channel method and the sudden approximation. Second, the calculations for the screening contribution based on these three models are in good agreement with experiment, within experimental uncertainties. This good agreement also occurs for the electron loss of He^+ by the other targets from Ref. [5].

However, some differences between these three models and the data can be observed. In the sudden approximation of Ref. [19], the possibility of multielectronic transitions occurring in the target atom concomitantly with the projectile loss is taken into account naturally. The constraint of the nonionization of the target atom during the collision is assumed in both the free-collision model and the coupled-channel method, so that the inclusion of the target ionization channel must be made *ad hoc*. This can be done, for instance, by combining the different collision channels within the independent electron model (IEM) [33]. Following this procedure, one can obtain the total loss cross section, including the target ionization channel, approximately as [19]

$$\sigma_{\text{loss}}^{\text{corr}} = [1 - P_I(0)]\sigma_{\text{screen}} + \sigma_{\text{anti}}, \qquad (4)$$

where $P_I(0)$ is the target ionization probability at zero impact parameter and σ_{anti} is the antiscreening contribution to

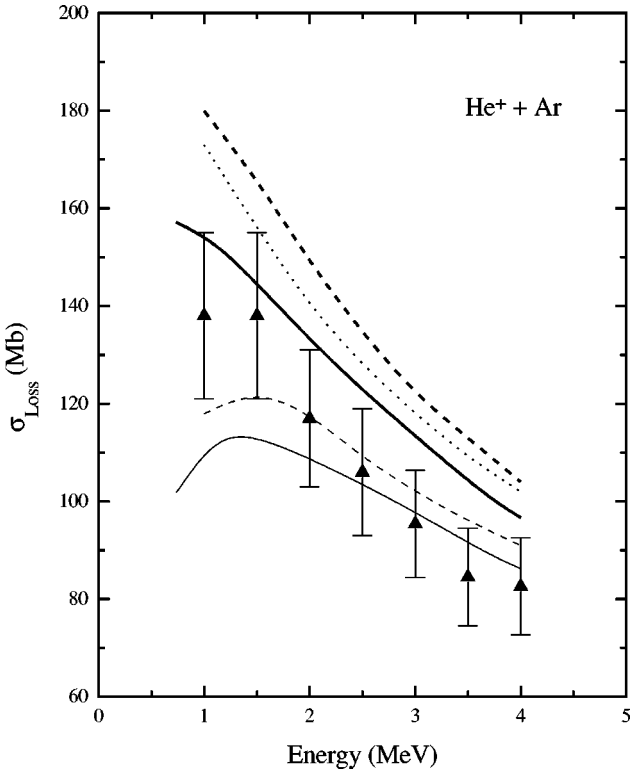

FIG. 2. Total electron-loss cross sections of He^+ by Ar as a function of the projectile energy. Experiment: triangles, Ref. [5]. Theory: thick-solid line, sum of screening [this work, Eq. (3)] and antiscreening (Ref. [25]) without correction for the target ionization; thin solid line, sum of screening [this work, Eq. (3)] and antiscreening (Ref. [25]), with correction for the target ionization [Eq. (4)]; thick dashed line, sum of screening (sudden approximation, Ref. [19]) and antiscreening (Ref. [25]) without correction for the target ionization; thin dashed line, sum of screening (sudden approximation, Ref. [19]) and antiscreening (Ref. [25]), with correction for the target ionization [Eq. (4)]; dotted line, sum of screening (coupled-channel method, Ref. [18]) and antiscreening (Ref. [25]).

the total loss cross section. The ionization probabilities were estimated from the semiclassical calculations of Hansteen *et al.* [34] for protons, with a Z_{eff}^2 scaling for the He^+ projectile, where Z_{eff} is a kind of effective charge of the He^+ ''seen'' by the target electrons. The value of Z_{eff}^2 was obtained by fitting Eq. (4) to the complete set of experimental data. In Ref. [19] this value was 1.8, while in the case of the free-collision model, a value of 1.6 was found. The corrected cross sections appear in Fig. 2 as the thin solid line (free-collision model) and the thin dashed line (sudden approximation [19]).

It can be seen that, with the inclusion of the target ionization channel, better agreement with experiment is obtained, both qualitatively and quantitatively. But discrepancies still remain for the lowest energies. This is due to the fact that the semiclassical calculations of Hansteen *et al.* are not expected to be realistic for low projectile velocities. Also, the simplification of using a single, average value for the projectile effective charge for the whole energy and target ranges may not be correct.

The total experimental electron-loss cross sections for C^{3+} and O^{5+} on Ar are shown in Figs. 3 and 4, respectively, as a function of the projectile energy, together with calcula-

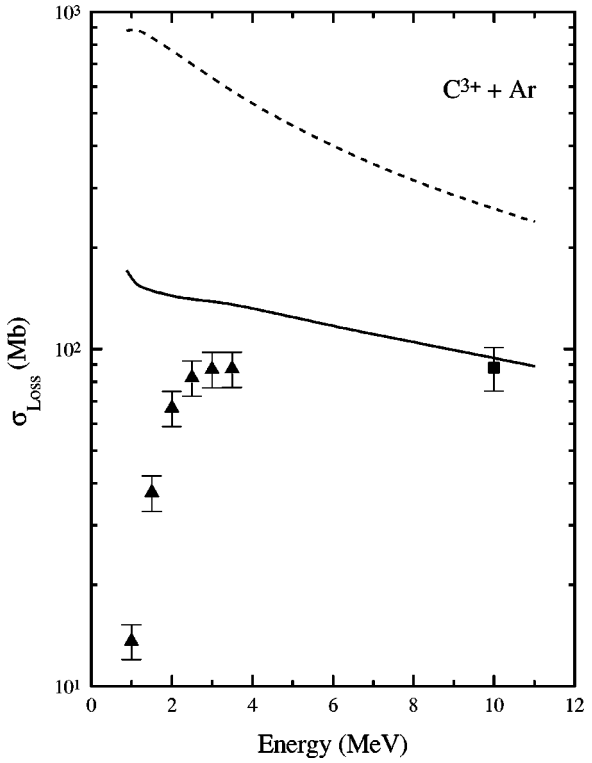

FIG. 3. Total electron-loss cross sections of C^{3+} by Ar as a function of the projectile energy. Experiment: triangles, this work; square, Ref. [20]. Theory: dashed line, sum of screening (PWBA) and antiscreening (Ref. [25]); solid line, sum of screening [this work, Eq. (3)] and antiscreening (Ref. [25]).

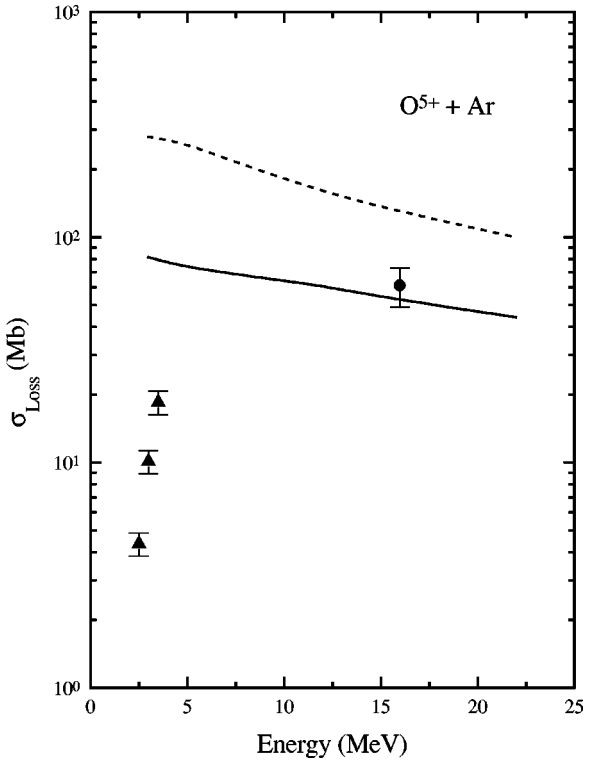

FIG. 4. Total electron-loss cross sections of O^{5+} by Ar as a function of the projectile energy. Experiment: triangles, this work; circle, Ref. [35]. Theory: dashed line, sum of screening (PWBA) and antiscreening (Ref. [25]); solid line, sum of screening [this work, Eq. (3)] and antiscreening (Ref. [25]).

tions using Eq. (3) and the PWBA for the screening contribution, both added to the PWBA extended sum-rule method of Montenegro-Meyerhof [25] calculations for the antiscreening. The experimental values obtained by Anholt *et al.* [20] (10-MeV C^{3+}) and Boman *et al.* [35] (16-MeV O^{5+}) are also included in Figs. 3 and 4, respectively. As can be readily seen from these figures, the low-energy results do not agree with the experiment, as they do in the He^{+} case, since in these velocity ranges, besides the target ionization, another competitive channel occurs in the collision, namely, the capture of a target electron by the projectile. This fact will be discussed in more detail later. Also, the velocity ranges of our experimental data lie close to the validity limits for the application of the free-collision model, mainly for the O^{5+} projectile. But for the high-energy data, the agreement is very good for both projectiles.

The improvement of the free-collision model when compared to first-order calculations is better shown when the behavior of the total electron-loss cross sections with the target atomic number is analyzed. This is done in Figs. 5, 6, and 7 for He^{+} (collision energy of 2.5 MeV), C^{3+} (collision energy of 3.0 MeV), and O^{5+} (collision energy of 3.5 MeV), respectively. Also included are the electron-loss cross sections of the He^{+} and C^{3+} projectiles by atomic hydrogen targets from Ref. [26]. The theoretical total electron-loss cross sections calculated using Eq. (3) (thick solid line) and the PWBA (screening) (dash-dotted line) are also presented in all these figures. In the He^{+} case, comparison is also made with total cross sections with the screening contribution calculated using the coupled-channel method from Ref. [18] (dotted line) and the sudden approximation [19] (thick dashed line). In both these works calculations are presented only up to the Kr target. In all the cases, the antiscreening contribution was calculated using the extended sum-rule method [25]. They are shown in Figs. 6 and 7 for C^{3+} and O^{5+}, respectively. It should be mentioned that the lines representing the theoretical values are only to guide the eye, since they join the points were the calculations were effectively performed (the vertices appearing in these lines).

First of all, one observes that the same saturation which appears in the experiment for the He^{+} projectile is also present for C^{3+} and O^{5+}. Second, as observed in Ref. [5], this saturation occurs in the first-order calculations for the antiscreening contribution, but not in those for the screening, in all cases. It can be noted that the calculations for the screening using the extended free-collision model [Eq. (3) above] provide total cross sections which are again close to the ones obtained in the sudden approximation [19] and with the coupled-channel method [18]. The quantitative agreement with the experimental data is very good for the He^{+} projectile up to the Ar target. For heavier targets, some discrepancies appear, which can reach 45% for Xe. As pointed out before, these can be attributed to the constraint of the nonionization of the target atom during the collision. When this correction is included in the calculations, better agreement with experiment is obtained, as can be seen in Fig. 5 for the free-collision model (thin solid line) and the sudden approximation (thin dashed line).

For the heavier — and higher-charged — C^{3+} and O^{5+} ions, the discrepancies between the calculations in the free-

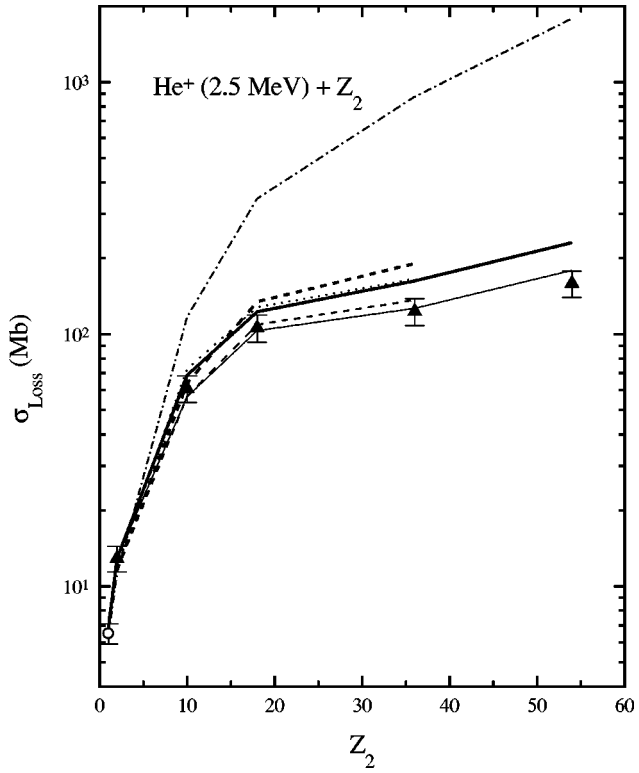

FIG. 5. Total electron-loss cross sections of 2.5-MeV He^+ as a function of the target atomic number. Experiment: triangles, Ref. [5]; open circle, Ref. [26]. Theory: dash-dotted line, sum of screening (PWBA) and antiscreening (Ref. [25]); thick solid line, sum of screening [this work, Eq. (3)] and antiscreening (Ref. [25]) without correction for the target ionization; thin solid line, sum of screening [this work, Eq. (3)] and antiscreening (Ref. [25]), with correction for the target ionization [Eq. (4)]; thick dashed line, sum of screening (sudden approximation, Ref. [19]) and antiscreening (Ref. [25]) without correction for the target ionization; thin dashed line, sum of screening (sudden approximation, Ref. [19]) and antiscreening (Ref. [25]), with correction for the target ionization [Eq. (4)]; dotted line, sum of screening (coupled-channel method, Ref. [18]) and antiscreening (Ref. [25]). The lines are only to guide the eye.

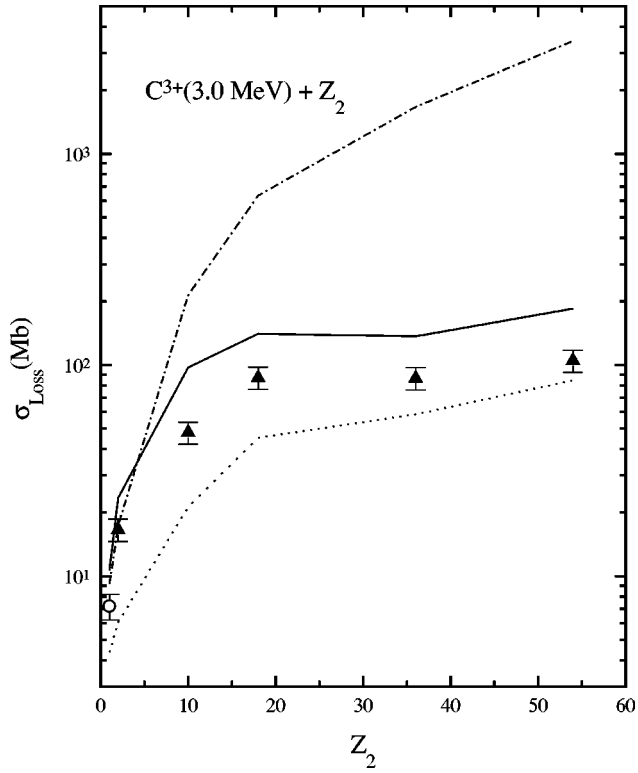

FIG. 6. Total electron-loss cross sections of 3.0-MeV C^{3+} as a function of the target atomic number. Experiment: triangles, this work; open circle, Ref. [26]. Theory: dash-dotted line, sum of screening (PWBA) and antiscreening (Ref. [25]); solid line, sum of screening [this work, Eq. (3)] and antiscreening (Ref. [25]). The antiscreening calculations from Ref. [25] are shown as the dotted line. The lines are only to guide the eye.

collision model and the experiment in the low-velocity region are larger: they lie between 35% and 80% for C^{3+} and factors of between 3 and 10 for O^{5+}. These discrepancies are in contrast with the good agreement presented in the case of the He^+ and also of the H^0 and H^- projectiles [24]. As mentioned before, they are due to the occurrence of other competitive collision channels and will be discussed in the end of this section.

The most important feature concerning the results presented in Figs. 5–7 is that the behavior of the screening contribution with increasing target atomic number when the extended free-collision model is used is the same as those of the experimental data and of the first-order calculations for the antiscreening, presenting the same saturation with increasing target atomic number. This was also observed by Riesselmann *et al.* in the electron-loss cross sections of both $H(1s)$ and H^- projectiles by noble gases [24]. The fact that both the screening and antiscreening contributions — and, consequently, the total cross section — present the same saturation with the target atomic number is remarkable, since these mechanisms have different origins and their dependences on the impact parameter of the collision are rather different within first-order models [3]. A possible explanation for the similar behavior observed here is the following. The extended free-collision model applied to the screening is based on the elastic cross sections for the (free) *electron* scattering by the target nucleus. However, as mentioned before, the requirement that the momentum transferred to the projectile-active electron during the collision must be such that it acquires enough energy to be ionized implies that, for kinematic reasons, the free-electron scattering angle θ (see Fig. 1) must be larger than a critical value, which is the lower limit for the integration on the scattering angle. This critical angle — which, according to Eq. (2), has a minimum value given by $(u_{\rm rms}/v_{\rm N})(\sqrt{2}-1)$ — is equivalent to considering an upper limit for the impact parameters which contribute effectively to the screening. The electron-scattering differential cross sections calculated by McCarthy *et al.* [32] present deep minima at some given angles, which implies that the value of θ_C with respect to these minima is very important. Also, the behavior of these differential cross section for a given electron velocity is such that they are large for small scattering angles, decreasing very rapidly as the angle increases. But the values of the cross sections at small angles for the Ar, Kr, and Xe targets are not very different from each other [32], varying at most linearly with Z_2. This means that, if the critical angle is small — which is the case when the collision velocity is greater than the root-mean-square velocity of the projectile active electron — the inte-

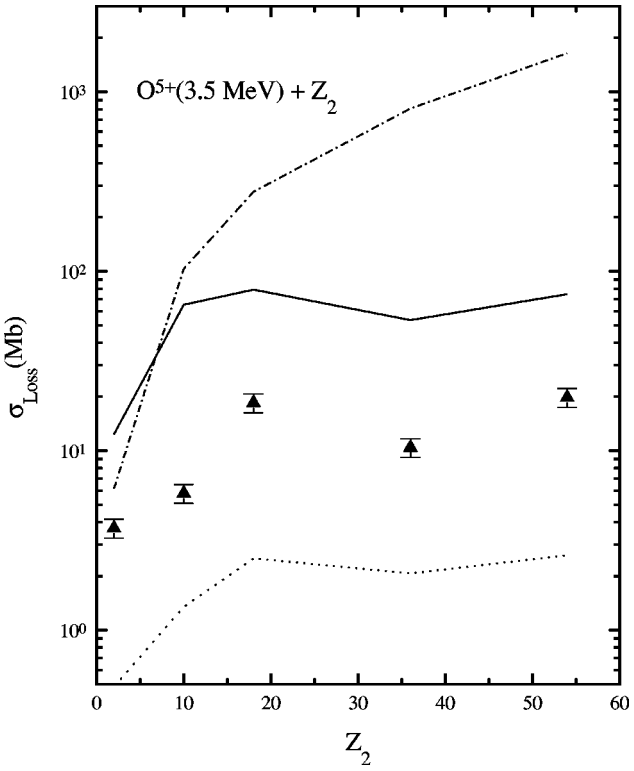

FIG. 7. Total electron-loss cross sections of 3.5-MeV O^{5+} as a function of the target atomic number. Experiment: triangles, this work. Theory: dash-dotted line, sum of screening (PWBA) and antiscreening (Ref. [25]); solid line, sum of screening [this work, Eq. (3)] and antiscreening (Ref. [25]). The antiscreening calculations from Ref. [25] are shown as the dotted line. The lines are only to guide the eye.

gration in θ of the differential cross section in Eq. (3) may give approximately the same result, irrespective of which target atom is considered, since the contributions from smaller angles (i.e., large impact parameters) to the integrals, which are the dominant ones, are approximately the same. This does not happen in the PWBA calculations for the screening, where the dominant contributions come from small impact parameters, which implies that the projectile electron ''sees'' a weakly screened target nucleus, so that the cross sections vary with the target atomic number as Z_2^n, with $1 \leqslant n \leqslant 2$.

The rather large differences between the cross sections calculated within the free-collision model and the experiment for the electron loss of C^{3+} and O^{5+} in the low-velocity regime are mainly due to the fact that two other processes compete as alternative exit channels to the collision. These are direct single or multiple ionization of the target atom and the single or multiple capture of target electron(s) by the projectile. As can be seen from Tables III–VI, in the velocity range considered here, the single capture can be up to three — and the double capture up to two — orders of magnitude larger than the loss cross sections. The importance of the direct ionization channel was already shown here for the He^+ projectile. Coincidence measurements of the direct ionization cross sections for the same targets as here by He^+ and C^{3+} projectiles also attest to its importance for these velocities [36]. Thus, the coupling of these competitive channels has to be taken into account for a correct description of the problem.

The lack of theoretical models which completely describe these processes in intermediate-velocity collisions of highly charged ions with heavy neutral atoms renders very difficult the evaluation of their contributions. However, the IEM can be used again to provide estimations for these contributions. This was done successfully by Montenegro *et al*. to analyze the electron loss of C^{3+} and O^{5+} projectiles by H_2 and He targets in the same energy range as here [1]. Following the procedure adopted by these authors, the total electron loss cross section $\sigma_{\rm loss}$ of a one-active-electron projectile by a neutral target, with N outer-shell active electrons, can be written as

$$\sigma_{\rm loss} = [1 - P_C(0) - P_I(0)]^N \sigma_{\rm screen} + [1 - P_C(0) - P_I(0)]^{(N-1)} \sigma_{\rm anti}, \tag{5}$$

where $P_C(0)$ is the electron capture probability at zero impact parameter.

Even the use of this simple approach is far from being an easy task for heavy atoms, since there are still no reliable ways to evaluate the direct ionization and electron capture probabilities as functions of the impact parameter. However, in order to verify whether the IEM can be employed to properly describe this case, Eq. (5) was used to fit the calculated values of $\sigma_{\rm screen}$ and $\sigma_{\rm anti}$ to the experimental $\sigma_{\rm loss}$, using the combined probability $P_C(0) + P_I(0)$ as a fitting parameter. The values of N were taken as 2 for the He and 8 for the other targets. The fitted values range from 0.06 to 0.8, presenting a steep decrease with increasing collision energy and a slow decrease with the target atomic number. These behaviors are in qualitative agreement with what was to be expected. The steep decrease with energy is characteristic of the capture channel, while the slowly varying dependence with the target atomic number can be explained by the use of the same number of target active electrons for $Z_2 \geqslant 10$.

IV. SINGLE-ELECTRON CAPTURE

The calculations of the single-electron capture cross sections were made according to two different approaches. The first one uses the closed general expression for the capture of a target electron, initially in a nl subshell, into a $n'l'$ subshell of the projectile given by Eichler [23]. Here, the extension to multielectron targets proposed by that author is used.

The second approach uses the semiclassical (SC) model developed by Ben-Itzhak *et al.* [27] for the calculation of the impact parameter dependence of the single-electron capture probability based on the classical capture model of Bohr and Lindhard [37]. After integration of the impact parameter probability, the total cross section for the capture of one target nl-subshell electron, σ_{nl}, can be written as

$$\sigma_{nl} = \frac{16}{3} \pi \frac{Z_1^3}{v_N^7} N_{nl} \left(\frac{Z_{2_{\rm eff}}^{nl}}{n} \right)^2, \tag{6}$$

where Z_1 is the projectile charge, n is the principal quantum number of the active electron, $Z_{2_{\rm eff}}^{nl}$ is the effective target charge of the nl subshell of the active electron, and N is the number of electrons in subshell nl. In the derivation of this equation, it was assumed that the single-capture probabilities

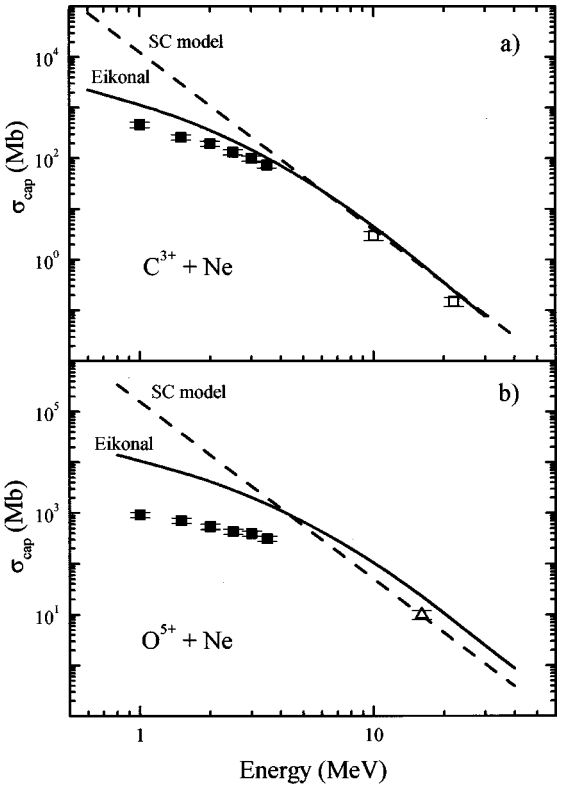

FIG. 8. Total single-electron capture cross sections as a function of the projectile energy for (a) C^{3+}, and (b) O^{5+} on Ne. Experiment: solid squares, this work; (a) open squares, Ref. [20]; (b) open triangle, Ref. [35]. Theory: dashed line, SC model [Eq. (6)]; solid line, total cross sections in the eikonal approximation (Ref. [23]).

are much larger than the double-capture ones in the velocity range studied, a fact that is confirmed by the experimental results presented in Tables III–VI. This analytical expression is valid when hydrogenic wave functions are used to describe the active electrons, which are here considered to lie in the outermost subshells of the target. Its derivation is presented in the Appendix.

Figure 8 compares the measured single-electron capture cross sections by C^{3+} [Fig. 8(a)] and O^{5+} [Fig. 8(b)] projectiles from Ne targets, presented in Table III and IV, respectively, with calculations using the eikonal approximation and Eq. (6), as a function of the collision energy. Also shown in these figures are the experimental data from Anholt *et al.* for C^{3+} [20] and from Boman *et al.* for O^{5+} [35] projectiles. The cross sections were calculated for n' varying from 2 (divided by 2, since both projectiles have one $2s$ electron) to 40, added up to all possible l' values in each shell. In all the calculations, the values of $Z^{nl}_{2_{\rm eff}}$ for the various targets and active-electron subshells from Clementi and Roetti [38] were used. As pointed out in Ref. [23], for multielectron targets a parameter θ, defined as the ratio between the ionization energy of the target active electron and $(Z^{nl}_{2_{\rm eff}}/n)^2/2$, should be used. The values of θ used here were also taken from Ref. [38]. In the case of the SC model, calculations were also performed using the Hartree-Fock $\langle r^{-1}\rangle_{nl}$ values from Ref. [39] (see Appendix). The differences in the calculated cross sections using these values and hydrogenic wave functions — Eq. (6) — are always smaller than 10%.

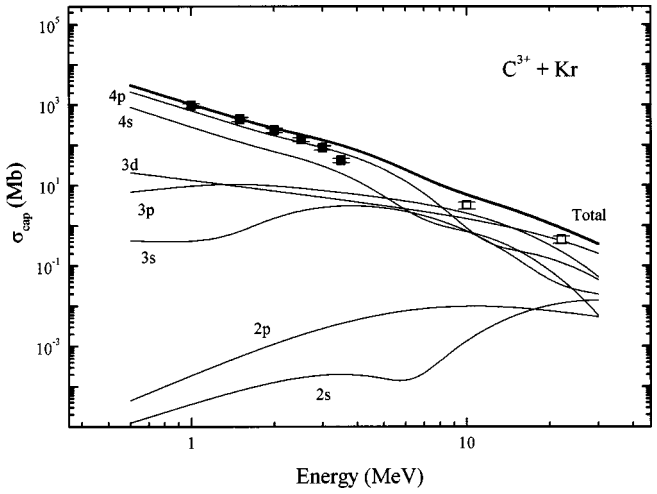

FIG. 9. Total single-electron capture cross sections as a function of the projectile energy for C^{3+} on Kr. Experiment: solid squares, this work; open squares, Ref. [20]. Theory: thick solid line, total cross sections in the eikonal approximation (Ref. [23]); thin solid lines, contributions from the target subshells in the eikonal approximation, as indicated (Ref. [23]).

In Fig. 9 the single-electron capture cross sections for a more complex system, namely, C^{3+} on Kr, is presented. The contributions to the total capture of the different subshells of Kr in the eikonal approximation are also shown. The $1s$ contribution does not appear in the figure since it is five orders of magnitude smaller than the $2s$ one.

The analysis of these figures shows that (i) the eikonal approximation gives better qualitative and quantitative descriptions of the data than the simpler SC model in the whole energy range and for all the systems studied; (ii) as expected, the agreement with the experiment is poorer for O^{5+} than for C^{3+}, since the O^{5+} projectiles are slower and lie closer to the limit of validity of the eikonal approximation; and (iii) the major contributions to the total cross sections from the different target subshells vary substantially within the intervals of projectile energies shown.

In Fig. 10 the measured capture cross sections of Table III by C^{3+} projectiles are presented as a function of the target atomic number and compared to calculations made with the two models described above. In the case of the eikonal approximation, calculations which include the contributions from all the possible subshells (solid line) and from only the last subshell (dotted line) are shown. Also included is the electron capture cross section from atomic hydrogen from Ref. [40]. It should be mentioned again that, as in the loss case, the lines representing the theoretical values are only to guide the eye. First of all, it can be seen that the data show the same saturation with increasing target atomic number as in the projectile-loss case, and that this saturation appears in the calculations with both models. But, again, the eikonal approximation presents a better agreement with the experiment than the SC model. It even shows the same kind of structure observed in the data between the Ne and Ar targets, although it provides values which can be up to 50% higher than the observed ones. It can also be noticed that, for this velocity, the relative importance of the contributions from the inner subshells increase with the target atomic number.

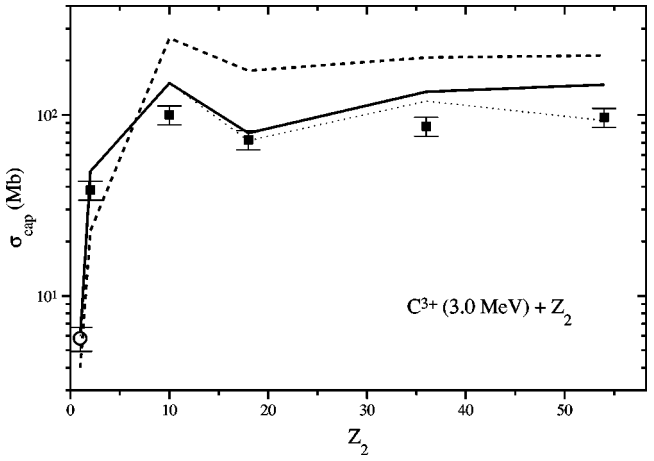

FIG. 10. Total single-electron capture cross sections of 3.0-MeV C^{3+} as a function of the target atomic number. Experiment: squares, this work; open circle, Ref. [40]. Theory: dashed line, SC model [Eq. (6)]; solid line, eikonal approximation with contributions from all possible target subshells (Ref. [23]); dotted line, eikonal approximation with the contribution of the last subshell only. The lines are only to guide the eye.

V. SUMMARY AND CONCLUSIONS

The main purpose of this paper is to present experimental data on electron-loss and single- and double-capture cross sections of C^{3+} and O^{5+} projectiles by noble gases in a velocity range that encompasses the antiscreening threshold. These data lie in a lower-velocity range than previous data and present the same saturation as the target atomic number increases which was observed before.

Furthermore, an extension of the free-collision classical-impulse approximation is presented and used to calculate the screening contribution to the total electron-loss cross sections. The comparison of these theoretical results with the data presented here, and also with the previous ones, shows a much better agreement than with first-order calculations for the screening contribution, including the saturation with the target atomic number. This was attributed to the fact that the free-collision model is a nonperturbative approach based on realistic elastic differential cross sections for the electron scattering by the target nucleus. Since these cross sections are dominated by the contributions from small scattering angles, that is, large impact parameters, the electron loss is caused by the almost completely screened potential of the target nucleus, in contrast with the predictions of first-order theories for the screening, where the dominant contribution comes from small impact parameters. However, first-order calculations for the antiscreening predict a much broader distribution of impact parameters contributing to the loss process. Thus, the calculations for the screening, using the free-collision approximation, and for the antiscreening, using the PWBA, present similar behaviors because both take into account contributions from approximately the same region of impact parameters.

However, in spite of the qualitative agreement with experiment, there still remains quite large quantitative discrepancies, which increase as the projectile charge increases. These were assigned to the competition with other collision exit channels, namely, the direct ionization of the target and the electron capture by the projectile, whose cross sections can be orders of magnitude higher than those for the loss in the velocity range of the present experiments. These channels must also be included in other theoretical models, such as the sudden approximation. A rough estimate of the contributions of these competitive channels within the independent electron model showed that their coupling, in a unitarized way, is mandatory to a complete description of the electron loss.

This fact becomes even more evident when one analyzes the single-electron capture data, which also present a saturation with the target atomic number. The closed analytical expression derived here for the total cross section from the capture probability in the semiclassical model of Ben-Itzhak *et al.* does not present good quantitative agreement with the experiment. On the other hand, a general expression for the $nl \rightarrow n'l'$ capture cross sections in the eikonal approximation gives a reasonable quantitative description of the data. However, it is not possible to extract the individual probabilities to be used within the IEM from this formulation.

ACKNOWLEDGMENTS

The authors would like to thank Professor Jörg Eichler for providing the FORTRAN computer code for the capture calculations in the eikonal approximation. This work was supported in part by the Brazilian agencies CNPq, FINEP, CAPES, FAPERJ, and MCT (PRONEX).

APPENDIX: SINGLE-ELECTRON CAPTURE IN THE SC MODEL

In this appendix, a simple analytical expression for the total cross sections of the single-electron capture of an electron in a *nl* subshell of the target atom is derived within the semiclassical model of Ben-Itzhak *et al.* [27] and the independent electron model [33]. In the following, it was assumed that the single-capture probabilities are much larger than the double-capture ones, so that these can be neglected.

In the semiclassical model proposed by Ben-Itzhak *et al.* [27], the probability of the capture of an electron, initially in subshell nl of a target of effective nuclear charge $Z_{2_{\rm eff}}$ and with a wave function ψ_{nlm}, by a projectile of charge Z_1 and velocity v_N as a function of the impact parameter b, $P_{C_{nl}}(b)$, is given by

$$P_{C_{nl}}(b) = \frac{2}{3}\frac{Z_{2_{\rm eff}}}{v_N} R_c \int_{V'} d\vec{r} |\psi_{nlm}|^2 \frac{1}{r}$$

$$= \frac{2}{3}\frac{Z_{2_{\rm eff}}}{v_N} R_c \sum_k c_{nl}^{(k)} \frac{d^k}{d\alpha_{nl}^k} I(\alpha_{nl}, b, R_C), \quad \text{(A1)}$$

where

$$I(\alpha_{nl}, b, R_C)$$

$$= \frac{4\pi R_C}{\alpha_{nl}} \begin{cases} \dfrac{1}{\alpha_{nl} R_C} - K_1(\alpha_{nl} R_C) I_0(\alpha_{nl} b) & (\text{if } b \leqslant R_c), \\ I_1(\alpha_{nl} R_C) K_0(\alpha_{nl} b) & (\text{if } b \geqslant R_c), \end{cases} \quad \text{(A2)}$$

with $\alpha_{nl}=2Z_{2_{\rm eff}}$, $R_c=2Z_1/v_N^2$, and I_0, I_1, K_0, and K_1 are modified Bessel functions [41]. The integral in Eq. (A1) is performed over a cylindrical volume V' with radius R_C around the projectile path. The $c_{nl}^{(k)}$ coefficients can be obtained from the radial electron density as follows [27]:

$$\rho_{nl}(r)=\sum_k c_{nl}^{(k)}\frac{d^k}{d\alpha_{nl}^k}\exp(-\alpha_{nl}r) \tag{A3}$$

and

$$\rho_{nl}(r)=\frac{1}{2l+1}\sum_m |\psi_{nlm}(\vec{r})|^2=\frac{1}{4\pi}|R_{nl}(r)|^2. \tag{A4}$$

The total capture cross section of an electron in the nl subshell, containing N_{nl} electrons, of a multielectron target, σ_{nl}, at high velocities, can be then approximately written as

$$\sigma_{nl}=N_{nl}\int_0^\infty P_{C_{nl}}(b)2\pi b db. \tag{A5}$$

Substituting Eq. (A1) into the above expression one finds

$$\sigma_{nl}=N_{nl}\frac{4\pi}{3}\frac{Z_{2_{\rm eff}}}{v_N}R_c\sum_k c_{nl}^{(k)}\frac{d^k}{d\alpha_{nl}^k}\int_0^\infty I(\alpha_{nl},b,R_C)b db. \tag{A6}$$

The integral appearing in the above equation can be easily done when Eq. (A2) is used and is equal to $(4\pi^2R_C^2)/(\alpha_{nl}^2)$. Thus, the total cross section can be written as

$$\sigma_{nl}=N_{nl}\frac{8\pi^2}{3}\frac{Z_{2_{\rm eff}}}{v_N}R_C^3\sum_k c_{nl}^{(k)}\frac{d^k}{d\alpha_{nl}^k}\frac{1}{\alpha_{nl}^2}. \tag{A7}$$

On the other hand,

$$\left\langle\frac{1}{r}\right\rangle_{nl}=\int_V d\vec{r}|\psi_{nlm}|^2\frac{1}{r}=\int_0^\infty |R_{nl}(r)|^2 r dr, \tag{A8}$$

where the integral is now made over the whole space.

But from Eq. (A4),

$$\int_0^\infty |R_{nl}(r)|^2 r dr=4\pi\int_0^\infty |\rho_{nl}(r)|^2 r dr. \tag{A9}$$

Substituting Eq. (A3) into the last result, one gets, after a straightforward integration,

$$4\pi\sum_k c_{nl}^{(k)}\frac{d^k}{d\alpha_{nl}^k}\frac{1}{\alpha_{nl}^2}=\left\langle\frac{1}{r}\right\rangle_{nl} \tag{A10}$$

and, thus,

$$\sigma_{nl}=N_{nl}\frac{16\pi}{3}\frac{Z_1^3Z_{2_{\rm eff}}}{v_N^7}\left\langle\frac{1}{r}\right\rangle_{nl}, \tag{A11}$$

where the definition of R_C was used.

Equation (A11) provides a simple analytical expression for the evaluation of single-capture cross sections. The values of $\langle r^{-1}\rangle_{nl}$ can be obtained, for instance, by means of either Hartree-Fock or hydrogenic wave functions. When the latter are used, one gets

$$\sigma_{nl}=\frac{16}{3}\pi\frac{Z_1^3}{v_N^7}N_{nl}\left(\frac{Z_{2_{\rm eff}}^{nl}}{n}\right)^2, \tag{A12}$$

which is Eq. (6) of the main text.

[1] E. C. Montenegro, G. M. Sigaud, and W. E. Meyerhof, Phys. Rev. A **45**, 1575 (1992).

[2] J. H. McGuire, N. Stolterfoht, and P. R. Simony, Phys. Rev. A **24**, 97 (1981).

[3] E. C. Montenegro, W. E. Meyerhof, and J. H. McGuire, Adv. At., Mol., Opt. Phys. **34**, 249 (1994).

[4] E. C. Montenegro, W. E. Meyerhof, J. H. McGuire, and C. L. Cocke, in *The Physics of Electronic and Atomic Collisions — XIX International Conference*, edited by L. J. Dubé, J. B. A. Mitchell, J. W. McConkey, and C. E. Brian, AIP Conf. Proc. No. 360 (AIP, New York, 1995), p. 515,

[5] M. M. Sant'Anna, W. S. Melo, A. C. F. Santos, G. M. Sigaud, and E. C. Montenegro, Nucl. Instrum. Methods Phys. Res. B **99**, 46 (1995).

[6] G. M. Sigaud, F. S. Jorás, A. C. F. Santos, E. C. Montenegro, M. M. Sant'Anna, and W. S. Melo, Nucl. Instrum. Methods Phys. Res. B **132**, 312 (1997).

[7] B. Brendlé, R. Gayet, J. P. Rozet, and K. Wohrer, Phys. Rev. Lett. **54**, 2007 (1985).

[8] K. Wohrer, A. Chetioui, J. P. Rozet, A. Jolly, F. Fernandez, C. Stephan, B. Brendlé, and R. Gayet, J. Phys. B **19**, 1997 (1986).

[9] X. -Y. Xu, E. C. Montenegro, R. Anholt, K. Danzmann, W. E. Meyerhof, A. S. Schlachter, B. S. Rude, and R. J. McDonald, Phys. Rev. A **38**, 1848 (1988).

[10] B. Sulik, N. Stolterfoht, S. Ricz, I. Kádár, L. Xiao, G. Schiwietz, P. Grande, R. Köhrbrück, K. Sommer, and M. Grether, in *Proceedings of the XVIII International Conference on The Physics of Electronic and Atomic Collisions, Aarhus, 1993*, edited by T. Anderson, B. Fastrup, F. Folkman, and H. Knudsen, p. 528.

[11] M. Chabot, K. Wohrer, A. Chetioui, J. P. Rozet, A. Touati, D. Vernhet, M. F. Politis, C. Stephan, J. P. Grandin, A. Macias, F. Martin, A. Riera, J. L. Sanz, and R. Gayet, J. Phys. B **27**, 111 (1994).

[12] U. Tiwari, A. K. Saha, L. C. Tribedi, M. B. Kurup, P. N. Tandon, and L. Gulyas, Phys. Rev. A **58**, 4494 (1998).

[13] U. Thumm, J. S. Briggs, and O. Schöller, J. Phys. B **21**, 833 (1988).

[14] T. Mukoyama and C. D. Lin, Phys. Lett. A **141**, 138 (1989).

[15] V. D. Rodriguez and J. E. Miraglia, Phys. Rev. A **39**, 6594 (1989).

[16] T. Mukoyama and C. D. Lin, in *Proceedings of the IX International Conference on the Physics of Highly Charged Ions, Bensheim, 1998*, edited by P. H. Mokler and S. Lüttges, p. 113.

[17] H. R. J. Walters, J. Phys. B **8**, L54 (1975).
[18] P. L. Grande, G. Schiwietz, G. M. Sigaud, and E. C. Montenegro, Phys. Rev. A **54**, 2983 (1996).
[19] A. E. Voitkiv, G. M. Sigaud, and E. C. Montenegro, Phys. Rev. A **59**, 2794 (1999).
[20] R. Anholt, X. -Y. Xu, Ch. Stoller, J. D. Molitoris, W. E. Meyerhof, B. S. Rude, and R. J. McDonald, Phys. Rev. A **37**, 1105 (1988).
[21] J. Eichler and F. T. Chan, Phys. Rev. A **20**, 104 (1979).
[22] F. T. Chan and J. Eichler, Phys. Rev. A **20**, 1841 (1979).
[23] J. Eichler, Phys. Rev. A **23**, 498 (1981).
[24] K. Riesselmann, L. W. Anderson, L. Durand, and C. J. Anderson, Phys. Rev. A **43**, 5934 (1991).
[25] E. C. Montenegro and W. E. Meyerhof, Phys. Rev. A **43**, 2289 (1991).
[26] M. M. Sant'Anna, W. S. Melo, A. C. F. Santos, G. M. Sigaud, E. C. Montenegro, M. B. Shah, and W. E. Meyerhof, Phys. Rev. A **58**, 1204 (1998).
[27] I. Ben-Itzhak, A. Jain, and O. L. Weaver, J. Phys. B **26**, 1711 (1993).
[28] E. C. Montenegro, W. S. Melo, W. E. Meyerhof, and A. G. de Pinho, Phys. Rev. Lett. **69**, 3033 (1992).
[29] E. C. Montenegro, W. S. Melo, W. E. Meyerhof, and A. G. de Pinho, Phys. Rev. A **48**, 4259 (1993).
[30] H. P. Hülskötter, W. E. Meyerhof, E. Dillard, and N. Guardala, Phys. Rev. Lett. **62**, 2261 (1989).
[31] I. S. Dmitriev and V. S. Nikolaev, Sov. Phys. JETP **17**, 447 (1963).
[32] I. E. McCarthy, C. J. Noble, B. A. Phillips, and A. D. Turnbull, Phys. Rev. A **15**, 2173 (1977).
[33] J. H. McGuire, *Electron Correlation Dynamics in Atomic Collisions* (Cambridge University Press, New York, 1997), Chap. 4.
[34] J. M. Hansteen, O. M. Johnsen, and L. Kocbach, At. Data Nucl. Data Tables **15**, 315 (1975).
[35] S. A. Boman, E. M. Bernstein, and J. A. Tanis, Phys. Rev. A **39**, 4423 (1989).
[36] A. C. F. Santos, W. S. Melo, M. M. Sant'Anna, G. M. Sigaud, and E. C. Montenegro (unpublished).
[37] N. Bohr and J. Lindhard, K. Dan. Vidensk. Selsk. Mat. Fys. Medd. **28(7)**, 1 (1954).
[38] E. Clementi and C. Roetti, At. Data Nucl. Data Tables **14**, 177 (1974); D. Cruz-Garritz, J. A. Chamizo, and A. Garritz, *Estructura Atomica* (Addison-Wesley Iberoamericana, Wilmington, 1991), Chap. 8.
[39] C. F. Fischer, *The Hartree-Fock Method for Atoms* (Wiley, New York, 1977), Chap. 2.
[40] M. M. Sant'Anna, W. S. Melo, A. C. F. Santos, G. M. Sigaud, E. C. Montenegro, and M. B. Shah (unpublished).
[41] F. W. J. Olver, in *Handbook of Mathematical Functions*, edited by M. Abramowitz and I. A. Stegun (Dover, New York, 1972), Chap. 9.